Modeling and Analysis of a High-Torque, Hydrostatic Actuator for Robotic Applications

JAMES E. BOBROW AND JAYESH DESAI
DEPARTMENT OF MECHANICAL ENGINEERING
UNIVERSITY OF CALIFORNIA, IRVINE
IRVINE, CALIFORNIA 92717

ABSTRACT

The goal of this research is to develop a robot actuator capable of producing and controlling large output torques. Because of friction and backlash, it is difficult to control large output torques if they are obtained from an electric motor through a gear train. If no gearing is used, it is possible to accurately control torque output, but large torques are not possible unless heavy direct-drive motors and high-powered current amplifiers are used. In this paper, we describe a pressure-controlled hydrostatic transmission which can be used as an alternative to a gear train. It uses a fixed-displacement hydraulic pump and rotary actuator to eliminate problems due to backlash, and enables large output forces or torques of an actuator to be accurately measured and controlled. An analog control system is used to achieve a desired force output, and a digital compensator is used to obtain position control. Modeling, simulations, and experiments are presented to describe the system and its capabilities.

This research was supported by Parker-Hannifin, Parker-Bertea Aerospace Division.

INTRODUCTION

In many of today's applications of robotics, there is a pervasive need for a system with a large load carrying capacity, that is light-weight, that has the ability to exert a specified force on its environment, and is relatively inexpensive. The key to improving robot performance is to improve the performance of their actuators. Several kinds of actuators are presently being used, including electric motors and hydraulic actuators.

Electric motors are used to drive most robot systems, using either direct-drive designs [Asada and Kanade, '87] or gear trains. Direct drive systems are the most straight-forward to control, but they are also very inefficient unless they are used with a mechanical linkage such as a parallel drive mechanism [Asada and Youcef-Toumi, '84]. The main problem is that motors deliver their peak power output at 1/2 their maximum angular velocity, and they are seldom used at this speed. They are usually operated a relatively slow speeds. Hence, direct-drive motors must be sized to handle large static torques, and then are seldom operated at their peak power output levels. Also the weight of the motor's themselves may introduce large loads for a manipulator to support.

One solution is to use a large speed reducer or gear train which allows the motor to be sized so that it operates more often at the speed that it is capable of producing its maximum power. Unfortunately, the nonlinearities of friction and backlash arising from speed reducers create major obstacles for control system designers. Even if the speed reducer has a minimum amount of friction and backlash there is still another problem. In many robot applications it is desirable to control the force that the actuator exerts on its environment. This requires that a strain gage and flexure be mounted to sense the output force. This increases the expense and complicates the design, and the added dynamics due to the flexure complicates the control system design. Example applications and designs of torque control systems for robots are given in [Luh, et. al. '81, Paul and Shimano '76, Pfeffer, et. al. '87, and Wu '85]. The use of force control for robot hands is discussed in Salisbury and Craig, '82.

Hydraulic servoactuators have been used for a number of years for both position and force control applications in aircraft, machine tools, and robots [Maskrey and Thayer '78, Blackburn et. al. '60]. The main advantage of these systems is the high power and force output levels they are capable of achieving. The main disadvantages are that they require a large external accumulator and pump, they require extensive plumbing from the accumulator to the actuators, and they use servovalves for control which are relatively expensive. However, even with these substantial disadvantages, they are prevalent in nearly every application where large forces or torques are required.

Recently, a self-contained hydraulic system has been developed termed an "electrohydrostatic actuator" [Parker Bertea Aerospace '88] that accomplishes the speed reduction of a gear train and has high position accuracy. It is capable of producing forces as large as 50000 lb and weighs a total of 30 lb. It requires no external accumulator and pump as needed in conventional servovalve controlled systems. In this paper we present experiments with a similar system which uses a rotary actuator to produce large output torques. It is fitted with pressure transducers on each side of the actuator, and this enables direct control of the output torque. A dynamic model of the nonlinear system is presented, and a pressure control system is simulated and tested experimentally. A position control design is also presented.

System Description and Model

Description. The system shown in Figure 1 consists of a brushless DC motor, a fixed displacement hydraulic pump, a small accumulator, and a rotary actuator. A rotary actuator was used rather than a linear one in order to compare its performance with that obtained from motors and gear trains.

A pulse-width-modulated current amplifier drives the brushless DC motor. The motor drives the pump, and depending on its direction of rotation, the pump forces fluid from side 1 to side 2 of the actuator or vice-versa. This causes motion of the rotary actuator in direct proportion to rotation of the pump, except for a small error due to leakage which occurs between the two sides of the pump and the two sides of the actuator. The fluid in the accumulator is pressurized with a small piston and spring to approximately 100 psi. When the pressure on either side of the actuator drops below the pressure in the accumulator, a one-way valve opens and fluid from the accumulator enters the system.

The key to successful operation of this system is this small accumulator and check valves. When the actuator forces a large, a sizable volume of fluid is compressed on the high pressure side of the actuator. If there were no accumulator, a void in the fluid would be created on the low pressure side of the pump, and it would no longer function properly. The accumulator and one-way valves provide fluid to the lines to make up for this compressibility and hence prevent cavitation.

In order to obtain light weight, a small displacement pump is used in conjunction with a motor capable of rotating at high angular velocities. If a high speed motor is used, a lower torque is required for a given power output. Hence, a smaller and lighter motor can be used. We experimented with several combinations of motors and pumps, and found that a 18000 rpm motor worked excellent, but needed large cooling fins to dissipate excess heat generated after prolonged use. For the experiments reported here, a larger 6000 rpm motor was used. Its peak torque output is 40 in-lb, and is geared down though this hydraulic transmission with a ratio of 484.7:1 to produce a theoretical peak torque of 19388 in-lb and a maximum speed of 12.4 rpm. The actual peak torque was limited to about 7300 in-lb (600 ft-lb) because of pressure limitations (2000 psi) on the internal seals of the rotary actuator used in the experiments (it was a standard rotary actuator, [Parker-Hannifin '85]).

Dynamic Model. To develop a force (pressure) control system, a dynamic model of the hydraulic system is required. Consider the dynamics of the motor-amplifier combination. Because the amplifier senses and controls the motor current, the bandwidth (response time) of the motor is much higher than that of the overall system. Therefore, we assume that the torque output from the motor is directly proportional to the voltage input to the amplifier,

$$T_p(t) = k_1 v(t) \tag{1}$$

where T_p is the torque from the motor windings applied to the pump and motor armature, v is the voltage input to the amplifier, and k_1 is a proportionality constant.

Next consider the dynamics of the pump. If we assume that there is no friction or leakage in the pump, the power delivered to the pump from the motor is $T_p\dot{\theta}$, where θ is the angular displacement of the motor, and the dot indicates derivative with respect to time. The power delivered by the pump is Δpq, where $\Delta p = p_2 - p_1$ is the pressure difference across the lines, and q is the fluid flow rate through the pump. For the ideal system which is not accelerating and has no power loss,

$$T_p\dot{\theta} = \Delta pq. \tag{2}$$

The volumetric displacement D, which is the ratio of the flow rate through the pump to the angular velocity of the pump, is given by $D = \frac{q}{\dot{\theta}}$. Hence, for an ideal system that is not accelerating and has no leakage

$$T_p = \Delta pD. \tag{3}$$

For a realistic model, leakage and friction must be accounted for. The torque exerted on the motor armature and pump must overcome friction and the torque due to the pressure difference across the pistons in (3). The excess torque, if any, will

accelerate or decelerate the pump. A good model for the dynamics of the motor and pump assembly is [Merrit '67]

$$T_p = D\Delta p + b\dot{\theta} + \left(T_s + f(p_1 + p_2)\right)\frac{\dot{\theta}}{|\dot{\theta}|} + J\ddot{\theta}. \tag{4}$$

where J is the inertia of the coupled pump and motor rotors, b is the coefficient of viscous friction, T_s is the Coulomb friction due to the seals and bearings, and $f(p_1+p_2)$ is a Coulomb friction term which increases linearly with pressure.

Because of the high pressures and forces obtained from the pump, the compressibility of the fluid must be modeled. Compressibility is defined as the change in volume V per unit volume for a unit change in pressure p. Bulk modulus β, which is the reciprocal of compressibility, is given by $\beta = -V\frac{dp}{dV}$. Hence, the rate of change of pressure is related to the bulk modulus by

$$\dot{p} = -\frac{\beta}{V}\dot{V}, \tag{5}$$

where we have assumed the pressure increases uniformly throughout V.

The volume of fluid on either side of the pump is

$$V_1(\alpha) = V_{ms} - \frac{r^2 d}{2}\alpha, \tag{6}$$

$$V_2(\alpha) = V_{ms} + \frac{r^2 d}{2}\alpha, \tag{7}$$

where r is the radius of the actuator, d is the depth of the actuator, V_{ms} is the volume of fluid in the actuator and in the lines in the mid-stroke position, and α is angular position of the rotary actuator measured from the mid-stroke position. The change in fluid volume $\dot{V}$ in (5) is due to flow from the pump and to motion of the actuator. For side one, $\dot{V} = \dot{V}_1 + q_1$, where q_1 is the flow exiting the actuator (entering the pump). Using (5) and (6), the pressure equation for side one is

$$\dot{p}_1 = -\frac{\beta}{V_1(\alpha)}(q_1 - \frac{r^2 d}{2}\dot{\alpha}). \tag{9}$$

Similarly for side 2

$$\dot{p}_2 = -\frac{\beta}{V_2(\alpha)}(q_2 + \frac{r^2 d}{2}\dot{\alpha}). \tag{10}$$

For the ideal case, the fluid flow entering the pump equals that leaving it, or $D\dot{\theta} = q_1 = -q_2$. However, some leakage occurs in the pump which can be modeled by [Merrit '67]

$$q_1 = D\dot{\theta} - c_I(p_2 - p_1) + c_E(p1 - p3) \tag{11}$$

$$q_2 = -D\dot{\theta} + c_I(p_2 - p_1) + c_E(p2 - p3), \tag{12}$$

where c_I determines the internal cross-port leakage from side one to side two, and c_E gives the external leakage to the accumulator. Substituting these flow equations into (9) and (10) gives

$$\dot{p}_1 = -\frac{\beta}{(V_{ms} - \frac{r^2 d}{2}\alpha)}(D\dot{\theta} - c_I(p_2 - p_1) + c_E(p1 - p3) - \frac{r^2 d}{2}\dot{\alpha}) \tag{13}$$

and

$$\dot{p}_2 = -\frac{\beta}{(V_{ms} + \frac{r^2 d}{2}\alpha)}(-D\dot{\theta} + c_I(p_2 - p_1) + c_E(p2 - p3) + \frac{r^2 d}{2}\dot{\alpha}). \tag{14}$$

The rotary actuator drives a one-link arm, with the equation of motion

$$J_a\ddot{\alpha} = k_2(p_2 - p_1) - mgl\cos\alpha, \tag{15}$$

where J_a is the moment of inertia of the arm about the fixed pivot, m is the mass of the arm, l is the distance from the pivot to the center of mass, and the term $k_2(p_2 - p_1)$ gives the torque on the arm from the pressure difference Δp across the rotary actuator.

The nonlinear equations given by (4), (13), (14), and (15) represent the dominant dynamics for the motor/piston/actuator system. Because (4) and (15) are second order, a total of six states are needed to simulate the system. In the simulations of these equations, the six states were chosen as $\theta, \dot{\theta}, \alpha, \dot{\alpha}, p_1$, and p_2. We note that the three main assumptions used to obtain this model are: a) the DC motor dynamics are negligible, or, the motor torque is directly proportional the the amplifier voltage; b) the fluid compresses uniformly on either side of the actuator, which means that the pressure is constant throughout the volume; and c) idealized models were used for friction and leakage in (4), (13), and (14).

Determining the System Parameters. Before simulating the pressure control system, the constants used in the equations of motion are needed. We determined the constants either experimentally or from manufacturer's specifications as listed in Table 1. To determine the Coulomb friction in the pump T_s, the minimum voltage required to turn the motor was found experimentally. To determine b in (4), a valve connecting the two pressure sides was opened to make the pressure on both the sides equal at all times. The amplifier was given a constant voltage, and time was allowed for the system to reach a steady-state so that $\ddot{\theta} = 0$ and $\dot{\theta}$ is constant. Since $p_2 - p_1 = 0$, and assuming f is small, (4) shows that the torque supplied overcomes Coulomb friction and viscous friction. A number of readings were taken for different speeds and a plot of T_p versus $\dot{\theta}$ was made. The slope gives the constant b and the intercept is the value of T_s, which is a check for the previously calculated value. Explanation as to how we obtained the constants c_E and c_I is given in the following discussion of the open loop response.

OPEN AND CLOSED-LOOP EXPERIMENTS AND SIMULATIONS

By applying a step input voltage v to the motor amplifier in (1), the response of the open-loop (no feedback) system can be obtained. To investigate the behavior of the fluid model, the output shaft was clamped fixed at the midstroke position $\alpha = 0$. A constant voltage was input to the motor amplifier which creates a constant torque on the pump rotor. The resulting pressure Δp was input to the oscilloscope, and interesting behavior was observed for low input voltages. Erratic fluctuations in pressure occurred on the high pressure side of the actuator. The fluctuations are caused by alternating leakage an rotation of the pump. After a peak in pressure, the friction in the pump and seals holds the rotor stationary until the pressure drops low enough for the constant input torque to cause the pump to rotate once again.

To simulate the behavior, we adjusted the values of c_E and c_I in (11) and (12) until our numerical solution agreed fairly well with the experimental response. An example simulation is shown in Figure 2. At higher input torques applied to the pump, the stick-slip phenomena described above did not occur. Figure 3 shows the experimental response and the simulated response to an input torque of 10 in-lb. The noise in the experimental response is due to problems with the pressure transducer amplification electronics. The behavior is analogous to the response of a mass-spring-damper due to a constant force input. The effective spring constant is due to the hydraulic fluid compressibility.

Analog pressure control. The fluctuations in the actuator output torque due to variations in pressure described in the last section are undesirable if the actuator is to be used for robotic applications. In many instances it is necessary to have control of the output torque from the actuator. For example, torque control is needed to exert a given force for an assembly operation or to cause a robot arm to follow a prescribed trajectory. To achieve torque control, an analog circuit was designed. An analog controller was used rather than a digital one because it allows for a natural separation between the position controller and the force controller. In addition, the bandwidth of the pressure controller is an order of magnitude higher than the position controller so a higher sampling rate would have been needed for digital control.

We tested several controllers with experiments and simulations, and found that in order to obtain a fast response, a feedback compensator which performed well is

$$v = k_p\big((\Delta p_{ref} - \Delta p) - k_v\dot{\theta}, \tag{16}$$

where v is the voltage to the motor-amplifier in (1), Δp_{ref} is the desired pressure difference across the actuator, and the gains k_p, k_v were chosen experimentally as described below. Note that this compensator uses the state variables $\dot{\theta}, p_1$, and p_2, which corresponds to full state feedback if one does not control θ in (4), and α is held fixed. With this control law, the desired torque corresponding to Δp_{ref} is input to the system, and the actual output torque given by Δp is quickly driven to the desired value.

If the system given by (4), (13), and (14) were linearized for a given α, and no friction were assumed, full state feedback would allow arbitrary placement of the closed-loop poles for this system. Hence, any desired response time could be obtained. However, for the actual system, several limitations exist. The two most prominent factors which limit the performance of the pressure controller are the current (torque) limit of the

motor and amplifier, and the unmodeled dynamics of pressure waves in the hydraulic fluid. In (13) and (14), we assumed the pressure remains uniform throughout sides one and two. In reality, pressure waves travel through the lines at the speed of sound in oil when the pump operates. The natural frequency of the pressure waves was measured to be about 300 hz, and these waves are the source of some of the noise in our response plots.

Figures 4 and 5 show both experimental and simulated plots of the actual pressure output Δp and simulated output to a square wave and a sine wave command pressure Δp_{ref} in (16). To obtain these results, the pressure control law (16) was implemented on the experiment with analog electronics. The simulation included the motor saturation nonlinearity given by the constraint $\|T_p\| \leq 40.0$ in-lb. The values used for k_p and k_v were chosen experimentally to give a fast, stable response. The steady-state error could be eliminated using a small feed-forward term which changes linearly with Δp_{ref}.

Figures 6 and 7 show experimentally measured frequency response plots of the closed loop pressure controller for two fixed positions α of the rotary actuator. Although the system is nonlinear, the frequency response plots indicate that the dominant dynamics are approximately second order. The bandwidth of the pressure controller appears to be about $200/(2\pi) = 32$ hz.

Position control

Given the ability to control the torque applied to the actuator T_a with a relatively high bandwidth using the analog pressure controller of the last section, it is straightforward to design a position controller. We found that a simple PD digital compensator performed well. The control law was implemented digitally as

$$\Delta p_{ref}(t) = -c_1 e(t) - c_2/T(e(t) - e(t-T)) \tag{17}$$

where $e(t) = \alpha(t) - \alpha_{ref}(t)$ is the position error at time t, T is the sampling interval, α_{ref}, is the desired position of the arm, and the constants c_1, c_2 are the feedback gains for the position loop.

The control computer (an IBM PC) inputs the position α at time t, computes the desired command Δp_{ref} and outputs this value through a D/A converter to the analog pressure controller of (16). It is helpful to have an approximate linear model for this system in order to choose the gains c_1 and c_2. Figure 8 shows the model we used. For clarity, a model for an approximate continuous-time system is shown, even though the control loop was implemented digitally. In the figure, the closed-loop pressure control system is modeled as a second order linear system with $\omega_n = 150$ rad/sec and $\varsigma = .5$ which are roughly the values which match the results of the response curves in Figures 6 and 7 at low frequencies.

A root-locus plot is shown for this system in Figure 9, where it was assumed that the ratio $c_1/c_2 = 30$, and a variable gain g multiplies c_1 and c_2 to produce the plot. Note that the system is stable until $g = 770$, at which point the locus crosses the imaginary axis. More sophisticated controllers could be used to obtain a faster response, but this controller performed well for our application. Figure 10 shows the step response for the actual system with $g = 350$.

CONCLUSION

An alternative actuator to a motor and gear train has been presented which uses a hydrostatic transmission to enable large speed reductions and corresponding torque amplification. Problems due to friction and backlash in conventional gear trains are eliminated with the closed hydraulic system presented. A dynamic model of the system was developed, and it was shown that the output torque of the actuator can be controlled by sensing the pressure of the working fluid. Simulations and experiments were used to test the system and model.

REFERENCES

1 H. Asada and T. Kanade, "Design of Direct-Drive Arms," ASME Journal of Vibration, Stress, and Reliability in Design, Vol 105, No 3, 1983.

2 H. Asada and K. Youcef-Toumi, "Analysis and Design of a Direct-Drive Arm With a Five Bar Link Parallel Drive Mechanism," ASME Journal of Dynamic Systems, Measurement, and Control, Vol 106, No 3, pp 225-230, 1984.

3 J.F. Blackburn, G. Reethof, and J.J. Shearer, **Fluid Power Control**, Wiley, 1960.

4 J.Y.S. Luh, W.D. Fisher, and R.P. Paul, "Joint Torque Control by Direct Feedback for Industrial Robots," Proc. IEEE Conference on Decision and Control, pp 265-271, San Diego, Ca, 1981

5 R.H. Maskrey and W.J. Thayer, "A Brief History of Electrohydraulic Servomechanisms," ASME Journal of Dynamic Systems, Measurement, and Control, Vol 100, No 2, pp 110-116, June 1978.

6 E.H. Merrit, **Hydraulic Control Systems**, Wiley, 1967.

7 Parker Hannifin Inc, **Hydraulic and Pneumatic Rotary Actuators**, Catalog 1800-1, Cylinder Division, Des Plaines IL, 1985.

8 Parker Hannifin Inc, **Parker Bertea Aerospace, Electro Hydrostatic Actuator**, Control Systems Division, Irvine CA, 1988.

9 R. Paul and B. Shimano, "Compliance and Control," Proc. IEEE Joint Automatic Control Conference, pp 694-699, San Francisco, Ca, 1976

10 L. Pfeffer, O. Khatib, and J. Hake, "Joint Torque Sensory Feedback in the Control of a PUMA Manipulator," Proc. IEEE International Conference on Robotics and Automation, pp 1966-1971, Raleigh, NC, 1987.

11 J.K. Salisbury and J.J. Craig, "Articulated Hands: Force Control and Kinematic Issues," International Journal of Robotics Research, Vol 1, No 1, 1982.

12 C. H. Wu, "Compliance Control of a Robot Manipulator Based on Joint Torque Servo," International Journal of Robotics Research, Vol 4, No 3, pp 55-71, 1985.

Table 1: List of parameters used in the simulation.

Parameter	Value	Units	Method Determined
β	247,000	psi	from the specifications for the oil used
r	1.83	in	from actuator data
d	2.20	in	from actuator data
V_{ms}	3.16	in^3	from actuator data
D	.00796	in^3/rad	pump data
p_3	100.0	psi	preset
k_1	4.0	in-lb/volt	set by adjusting the amplifier gain
k_2	3.68	in-lb/psi	from the transmission ratio
J	0.03	lb-in-sec^2	from motor and pump data
J_a	23.3	lb-in-sec^2	from arm mass properties
T_s	4.0	in-lb	experimentally
b	0.01455	in-lb-sec	experimentally
c_E	6.5×10^{-6}	in^3/(sec-psi)	compared experiments to simulation
c_I	1.0×10^{-6}	in^3/(sec-psi)	compared experiments to simulation
T_{pmax}	40.0	in-lb	set by current limiting in amplifier
f	0.0	in-lb/psi	compared experiments to simulation

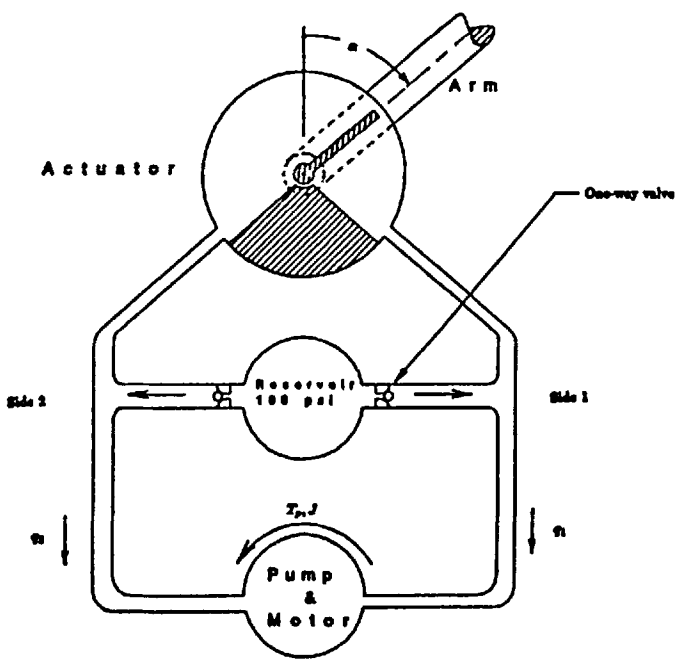

Figure 1: Test apparatus consisting of a DC motor, pump, small accumulator, and rotary actuator.

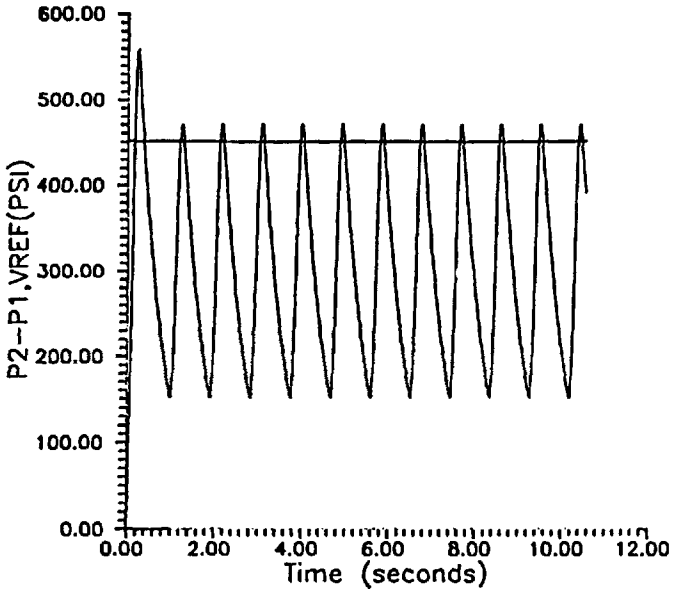

Figure 2: Simulation of open-loop stick-slip phenomenon at low pressures.

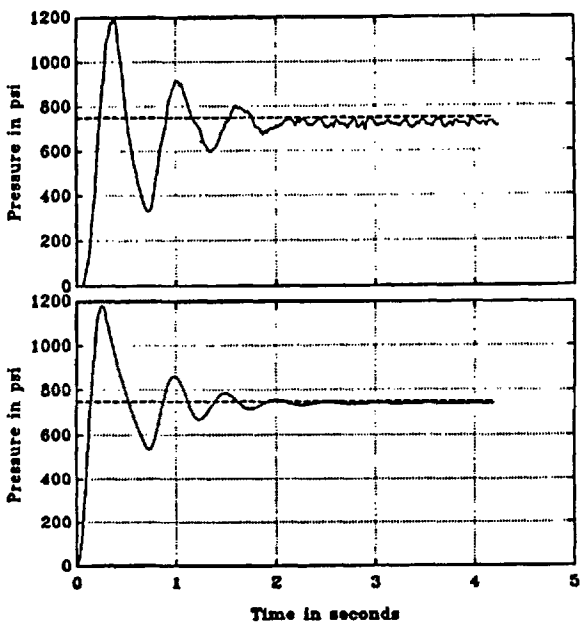

Figure 3: Experimental (upper plot) and simulated (lower plot) response of the open-loop system at higher pressures.

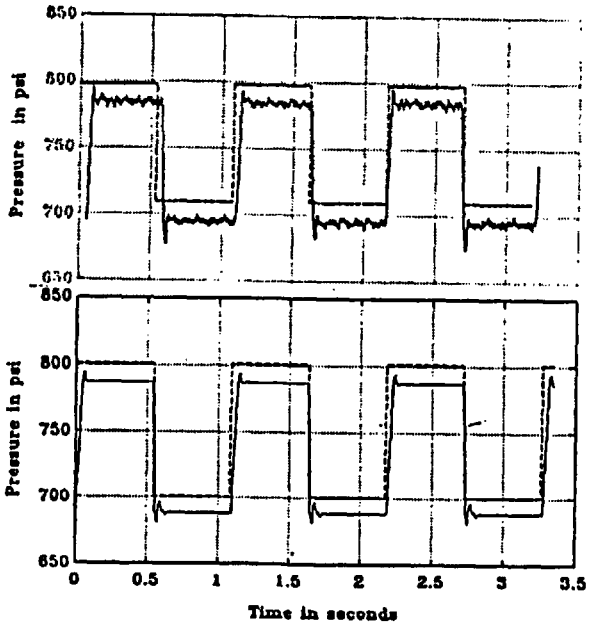

Figure 4: Experimental (upper) and simulated (lower) pressure response to a square wave reference input.

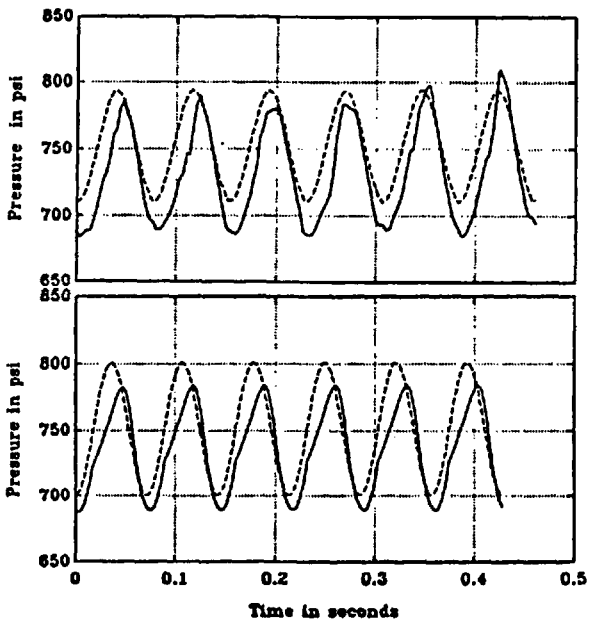

Figure 5: Experimental (upper) and simulated (lower) pressure response to a sine wave reference input.

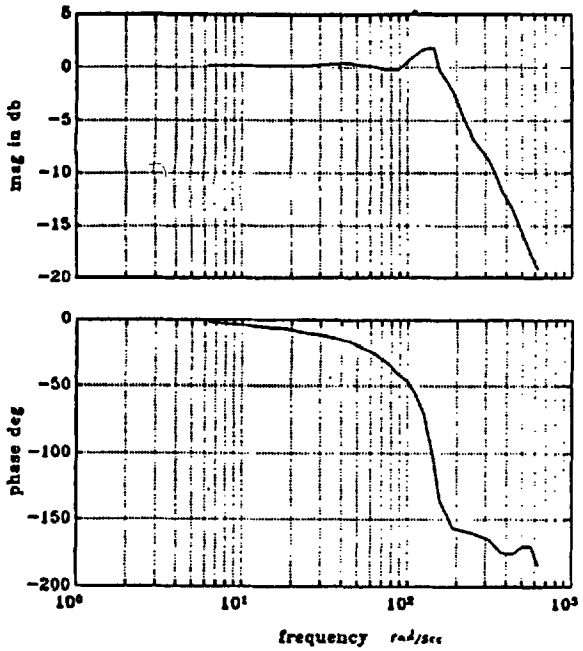

Figure 6: Experimental frequency response of the pressure control system when the actuator is in the midstroke position $\alpha = 0$.

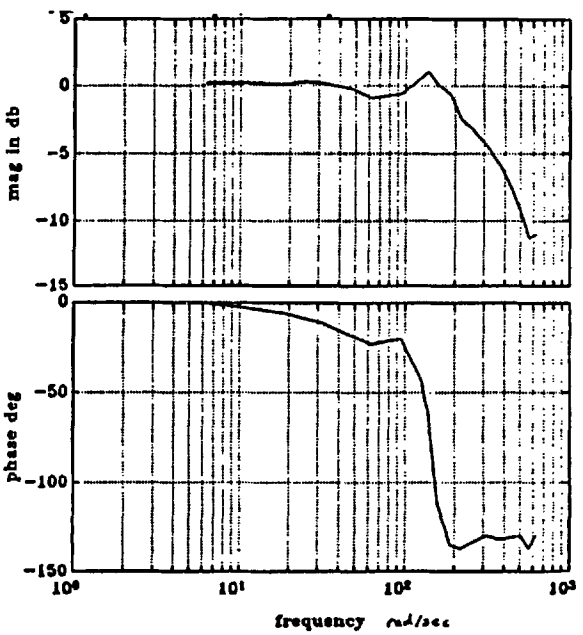

Figure 7: Experimental frequency response of the pressure control system when the actuator is moved 90 degrees $\alpha = \pi/2$.

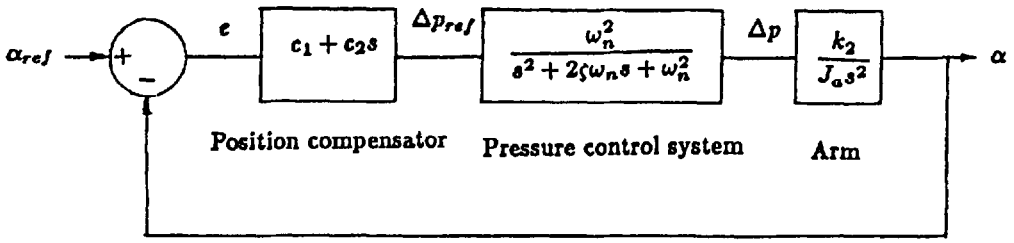

Figure 8: Block diagram of the overall position control system.

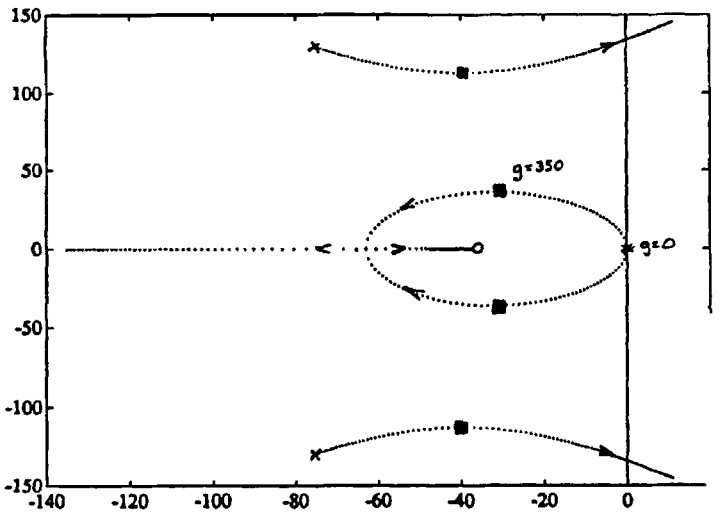

Figure 9: Root-Locus of the position control system with $c_1/c_2 = 30$.

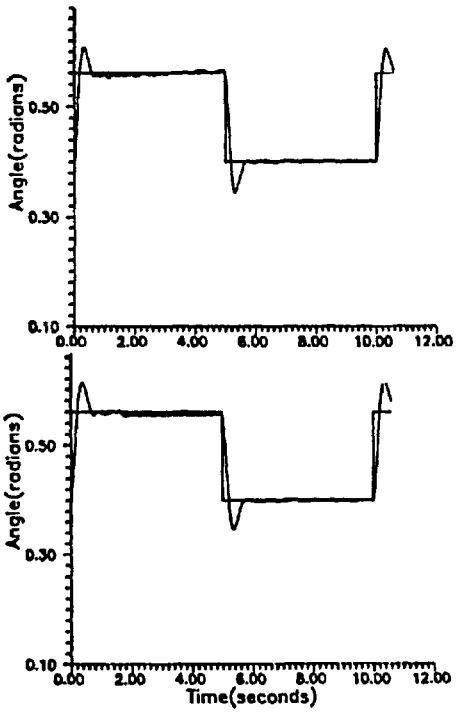

Figure 10: Experimental and simulated step response of the position control system.